Available online at www.sciencedirect.com
ScienceDirect
Journal of Nuclear Materials 362 (2007) 253–258
journal of nuclear materials
www.elsevier.com/locate/jnucmat

An X-ray absorption spectroscopy study of an oxide dispersion strengthened steel

M.A. Pouchon [a,*], A.J. Kropf [b], A. Froideval [a], C. Degueldre [a], W. Hoffelner [a]

[a] *Paul Scherrer Institute, Nuclear Energy and Safety, 5232 Villigen PSI, Switzerland*
[b] *Argonne National Laboratory, Chemical Engineering, 9700 S. Cass Avenue, Argonne, IL 60439, USA*

Abstract

Oxide dispersion strengthened (ODS) steels are being investigated as possible structural material for components of future nuclear power plants. The dispersoids in the matrix (yttria particles) serve as pinning points for moving dislocations, and thereby improve the creep behavior of the material. Depending on the product, the dimension of the particles is in the range from a few nm up to 100 nm. The material properties depend on the size distribution. It is also expected that other parameters of the dispersoids may influence the materials behavior. An extended X-ray absorption fine structure (EXAFS) study has been conducted on PM2000 (ferritic ODS steel) samples, in order to determine the structure of the yttria inclusions. A PM2000 sample, which had been irradiated with He ions of 1.5 MeV up to a matrix-damage of ~1 displacement per atom (dpa) in a surface layer of 2.7 μm in depth was measured. A multi angle implantation was performed, in order to avoid damage peaks as function of depth. A direct comparison of the EXAFS spectra and of the Fourier transformations shows no major difference between the irradiated samples and the non-irradiated one. Therefore any potential radiation induced damage or phase transformation of the dispersoids must be minor, which indicates good radiation stability under the given circumstances.

PACS: 28.41.Qb; 81.05.Ni; 61.10.Ht

1. Introduction

Oxide dispersion strengthened (ODS) steels are attractive candidate materials for high temperature applications where the creep resistance of conventional steels becomes an issue. The dispersoids in the tested material are nano-sized yttria particles, which are embedded in the steel matrix. These particles serve as pinning points for dislocations. For nuclear applications, a nickel-free ferritic matrix is advantageous, because of its reduced swelling behavior and the comparatively low activation potential. Therefore, this material possesses a good combination of properties for applications in the future generation of high temperature gas cooled nuclear reactors.

This article treats one aspect of the materials irradiation behavior using synchrotron radiation. With EXAFS it is possible to selectively investigate the structure of the yttria particles, although only being

* Corresponding author. Tel.: +41 (0)56 310 22 45; fax: +41 (0)56 310 35 65.
E-mail address: manuel.pouchon@psi.ch (M.A. Pouchon).

0022-3115/$ - see front matter © 2007 Elsevier B.V. All rights reserved.
doi:10.1016/j.jnucmat.2007.01.123

present in a very small fraction. It is therefore possible to find potential structural changes in the yttria particles that are induced by radiation. Results from an earlier investigation [1], which was performed on non-irradiated samples are taken as reference and compared to the EXAFS of a $^4He^{2+}$ irradiated sample.

2. Experimental

2.1. Material

The tested material is PM2000, a commercial ODS steel product from Plansee. It is composed of 73.5 wt% Fe, 20 wt% Cr, 5.5 wt% Al, 0.5 wt% Ti, and 0.5 wt% Y_2O_3, manufactured by mechanically alloying in a high energy mill to produce a solid solution which contains a uniform dispersion of yttria. The powder is consolidated using hot isostatic pressing followed by a hot and cold rolling procedure. A thermal treatment finalizes the production [2,3]. Yttria is present potentially in three phases, a cubic (α-phase, Ia$\bar{3}$), a hexagonal (β-phase, P$\bar{3}$m1) and a monoclinic (γ-phase, C2/m) one [4]. These represent the normal, the high-temperature and the high-pressure phases. As already stated in [1], the first and the latter seem to be the more probable ones, as they represent the normal case and the one, where due to matrix constraints, loads during production and/or surface tension of small particles, a high pressure is introduced. Additionally to the pure yttria particles, phases containing Al are reported in [5], these are mainly $YAlO_3$ as perovskite (YAP) and $Y_3Al_5O_{12}$ as garnet (YAG) structures.

2.2. Sample preparation and irradiation

Polished PM2000 samples were irradiated at the Swiss Federal Institute of Technology (ETH) in Zürich, using a tandem accelerator. Helium ions with a energy of 1.5 MeV are implanted under different incidence angles, in order to achieve a broader implantation profile, instead of a peak, which would result from a single energy and single incidence angle implantation. The damage profile was published earlier [6,7], but is also shown in Fig. 1 in the 'damage profile' box. In the earlier publications, the samples were irradiated with the purpose to find some swelling parameters and a change in hardness. Therefore the samples were covered with a transmission electron microcopy (TEM) grid, in order to generate an alternating pattern,

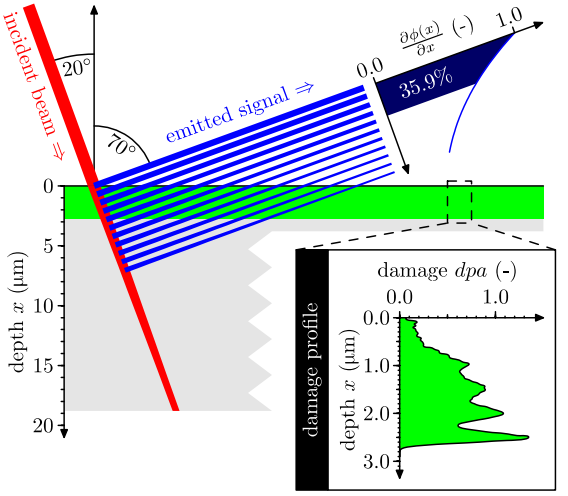

Fig. 1. EXAFS analysis of the irradiated sample. The incident beam hits the sample 20° off the surface-normal, or $\alpha_i = 70°$ to the surface. The emitted signal is analyzed orthogonally to it, and therefore 70° off the normal surface, or $\alpha_e = 20°$ relative to the surface. The beam thickness represents the non-absorbed X-ray part, and is therefore reducing in the material. The marked part from 0 to 2.7 μm in sample-depth represents the irradiated region, for which the damage is described in the box 'damage profile'. The fluence Φ of the emitted signal is normalized, and the fluence $\partial\Phi/\partial x$ for each infinitesimal layer is plotted right to the emitted signal. The integral over the depth region $x = [0, 2.7\ \mu m]$ is ~36% and is marked in the same plot. This represents the fraction of the EXAFS signal coming from the irradiated zone.

irradiated–non-irradiated region. Here the sample is fully irradiated on a surface of $4 \times 4\ mm^2$ to a total fluence of $5.6 \times 10^{16}\ cm^{-2}$, which corresponds to roughly 1 displacement per atom (dpa) for the addressed layer (or 0.6, if calculated according to [8], see also [7]). The so called addressed layer goes from 0 to 2.7 μm in depth (see again the damage profile shown in Fig. 1). The damage, which is discussed here, is an average value for the matrix with the particles being included. The displacement damage within the oxide particles is lower, because of the lower density and therefore lower cross section. This can be simulated using the TRIM (transport of ions in matter) code [9], as shown earlier in [1]. It must be mentioned here that the displacement energy for yttria is not very well known; the displacement energy directly influences the displacement damage calculated in the TRIM code.

2.3. EXAFS measurement

The irradiated sample was measured on the 10ID (MRCAT) beamline at the Advanced Photon Source (APS), Argonne National Laboratory.

Because of the shallowness of the irradiated layer, a steep analyzing angle of 70° relative to the sample surface, or 20° relative to the surface normal is chosen, the detector is positioned perpendicular to the incoming X-ray beam, and therefore faces the surface-normal with a angle of 70° (see Fig. 1). With this arrangement, the incoming beam propagates far into the sample, but the fluorescence signal is visible only from a shallower surface layer. Because of the quickly increasing travel path of $x/\cos(70)$ (with x being the depth of fluorescence source) through the material, a major part of the deeply emitted signal is absorbed. This study is focused on the yttria dispersoids, being responsible for the superior materials behavior of this ODS steel. These particles, only being present with 0.5 wt% in the matrix, are difficult to analyze using conventional techniques. Using EXAFS, the incident beam energy can be scanned across the absorption edge of yttria and therefore selectively analyze the dispersoids. The K edge of pure yttrium is 17038 eV and 17042 eV for yttria [10]. An analyzer crystal ($\Delta E \sim 105$ eV) was used to select only the $K\alpha_1$ and $K\alpha_2$ fluorescence lines at 14958.4 and 14882.9 eV. The absorption coefficient in pure Fe for the incoming X-ray beam is $\mu_i = 1/(31.68\ \mu m)$ and $\mu_e = 1/(22.12\ \mu m)$ for the $K\alpha_1$ emission (higher energy compared to $K\alpha_2$-line). Fig. 1 depicts the actual setup of this EXAFS measurement. The line thicknesses represent the beam fluence at the different positions in the sample. Because of the absorption mechanism, the line is thinning down with increasing propagation length. The same applies to the emitted signal, propagating toward the detector. The rays traveling a long path through the samples suffer greater absorption and are represented with thinner lines leaving the sample. The plot next to the emitted signal represents the photon fluence distribution, as a function of the emitting depth within the sample, which can be written as $\partial\phi(x)/\partial x$. The total emitted photon fluence ϕ is set to 100% and the integral photon fluence for the emitting region from 0 to 2.7 μm represents the fraction of the EXAFS part coming from the irradiated region.

For the absorption of the incoming beam and of the emitted signal, the Beer–Lambert–Bouguer law is applied with the appropriate absorption coefficients. The integral of the combined absorption of the incoming and the emitted signal is:

$$\phi(x) = \frac{\sin(\alpha_i)\sin(\alpha_e)}{\mu_i \sin(\alpha_e) + \mu_e \sin(\alpha_i)} e^{-x\frac{\mu_i \sin(\alpha_e) + \mu_e \sin(\alpha_i)}{\sin(\alpha_i)\sin(\alpha_e)}}.$$

Applied to the actual irradiation situation, this is:

$$\frac{\phi(2.7\ \mu m) - \phi(0)}{\phi(\infty)} = \sim 36\%,$$

which is the signal being emitted from the irradiated region.

The sample is measured at several locations. As described earlier, the irradiation is performed on a $4 \times 4\ mm^2$ squared region. EXAFS is taken in the center of this region. Additional measurements are taken 0.5, 1.0, 1.5 and 2.0 mm off-centre, with the last one reaching the border of the irradiated area. In this paper, the different data sets are generally denoted with their distance from the center, e.g., 0.0 mm, 0.5 mm, etc. All the measurements are performed at ambient temperature. To ensure a good statistics, for each sample position several scans are taken, these are: 9, 4, 5, 5 and 8 scans from center to the border.

As a reference for the non-irradiated sample, the experimental data already used in an earlier publication [1] is taken. This experiment was performed at the same light-source (APS), but using the 20BM-PNC-CAT beamline, at a temperature of 80 K.

2.4. EXAFS treatment

All data in this work were treated using the open source code ATHENA [11]. The Fourier transformation was performed with a k-weighting of 3 and a Hanning window, whose boundaries were set to $k = 2.5$–$12.5\ Å^{-1}$. The phase correction was conducted. The same treatment was also performed on the raw data of the unirradiated sample (which is the basis of [1]) in order to have comparability with the data from the irradiated sample. The data evaluation in [1] was carried out in a slightly different way, here a sine window was chosen with roughly 2.0 and $12.9\ Å^{-1}$ as boundaries. The result is however very similar (see Fig. 5 and [1]). The R-space cutoff between the background and the data was chosen at 1.2–1.4 Å (parameter *Rbkg* in ATEHNA), higher values would have resulted in nicer Fourier transformations but would clearly have been into the first edge, potentially altering the first shell amplitude.

3. Results

In the EXAFS analysis, the threshold energy for the absorption edge of yttrium is set to $E_0 = 17052.0$ eV in case of the reference sample.

This is comparable to the 17052.6 eV stated in [1]. The two different approaches to process the EXAFS data lead to similar values of E_0 for the reference sample. The energy shift in E_0 is thus not significant. For the irradiated samples, the E_0 is set to roughly 17050 eV. Any other yttrium oxide than Y_2O_3 is very unstable and unlikely. However, metallic yttrium can be identified on the EXAFS spectra as a small pre-edge around 17040 eV.

Fig. 2 shows the EXAFS spectra for each position on the irradiated sample. These represent the average curves of the scans taken at these positions. The single spectra are shifted in the ordinate for better visibility. The spectra are practically identical; only for large k are differences visible. Fig. 3 shows a comparison between the reference and the irradiated sample. The latter is the averaged curve from Fig. 2 and contains error-lines representing the standard deviation; here the differences for large k become visible again. For low k, the signal of the irradiated samples is less noisy because of the excellent statistics. The EXAFS spectrum of the reference sample is derived from only one scan. However, the smaller Debye–Waller factor (σ^2) for the low temperature measurement results in an increased amplitude of the high-k data.

Fig. 4 depicts the Fourier transformed data of the measurements shown in Fig. 2. As already mentioned, a Hanning window ranging from $k = 2.5$–$12.5\ \text{Å}^{-1}$ is chosen, and the phase correction is performed. The first peak exactly corresponds for all measurements. It is attributed to an O shell

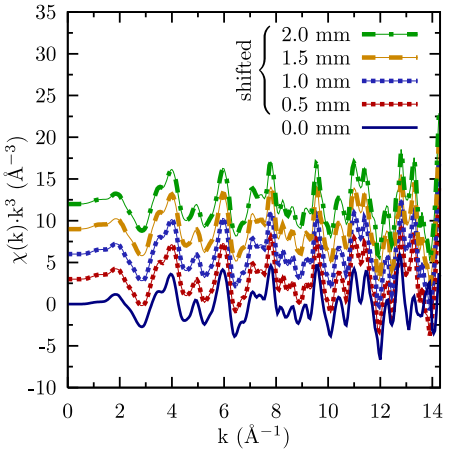

Fig. 2. EXAFS spectra of the irradiated region at ambient temperature, measured at the center (0.0 mm) and 0.5, 1.0, 1.5 and 2.0 mm from the center. Each off-center measurement is incrementally shifted by 4 Å^{-3} for better visibility.

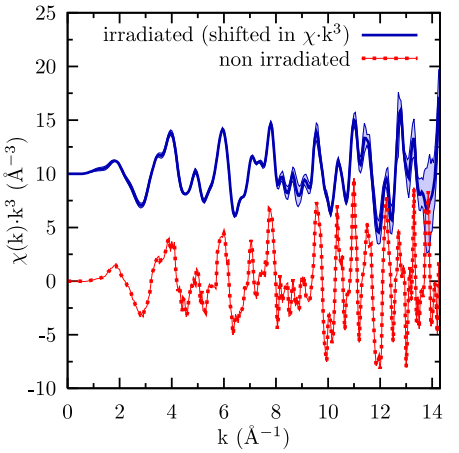

Fig. 3. Comparison of the EXAFS spectra measured on the reference sample (non-irradiated) and the irradiated sample. The data processing has been performed using the ATHENA software. The EXAFS spectrum of the irradiated samples represents an average of the spectra presented in Fig. 2, including two error lines which represent the standard deviation. The data of the irradiated sample is presented with an offset of 10 Å^{-3} in order to better distinguish the signals.

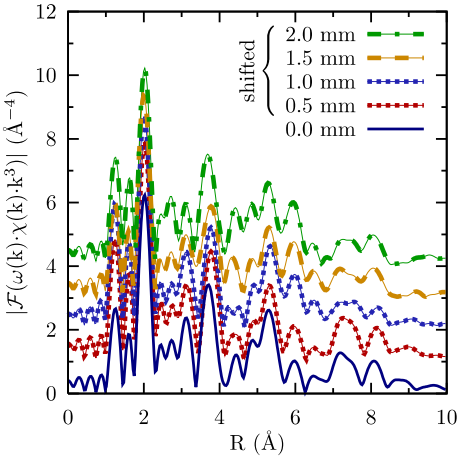

Fig. 4. Fourier transformation of the data displayed in Fig. 2. The Fourier transformed data is incrementally shifted by 2 Å^{-4} for better visibility.

around the absorbing yttrium atom (see the FEFF simulation in [1]). The succeeding shells are very similar, not showing any trend as a function of the position. Furthermore, Fig. 5 compares the Fourier transformed EXAFS signals for the irradiated and the reference samples. The comparison shows that the distribution is the same in both cases, although large amplitude differences are visible, likely due to a smaller σ^2. For $R > 6.5$ Å, differences become more pronounced, again due to the fact that the

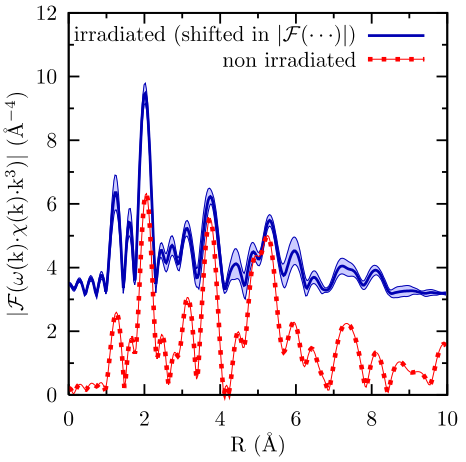

Fig. 5. Comparison of the Fourier transforms of the EXAFS signals presented in Fig. 3. The radial distribution function of the irradiated sample is again an averaged curve from the data presented in Fig. 4, including two error lines which represent the standard deviation. The data processing has been performed by using the ATHENA software. The data of the irradiated sample is presented with an offset of 3 Å^{-4}, in order to better distinguish the signals.

reference sample was measured at low temperature. The amplitude of the first peak, located at about 2 Å displays approximately the same intensity in both cases.

4. Discussion

As shown in the experimental section, more than one third of the signal comes from the shallow irradiated region. If the radiation changes the structure of the yttria it would be visible from this fraction of the signal. The measurements are very consistent, showing that for the chosen irradiation parameters, the oxide dispersion does not suffer any structural changes at ambient temperature.

In [1], TRIM simulations demonstrate the *dpa* distribution between the matrix and the included oxide particles. With these simple simulations it becomes clear, that the oxide particles suffer roughly a three times lower displacement damage than the matrix. In this case this signifies about 0.33 dpa within the yttria particles. Note that a dpa damage of 1.0 being introduced into the surrounding matrix has been investigated earlier [7], and clear damage of the matrix has been identified by TEM. A comparison with higher displacement damages promises to be interesting, potentially showing a threshold displacement damage where the irradiation changes the yttria structure.

Other ODS steels with different dispersion sizes may have different irradiation behavior. With a decreasing size, the chance of the particles being in a monoclinic phase increases. The irradiation behavior might change for the different structure, also changing the phase of some monoclinic particles into cubic. For smaller dispersoid particle sizes, beam intermixing of the yttria with its steel environment might become an irradiation issue.

The temperature chosen for the irradiation process might also influence this result. When changing the condition from ambient to elevated temperatures, helium bubble formation will play a role. When bubbles are formed at or near the yttria particles, some structural changes may well become visible.

5. Conclusions

Up to the tested radiation dose, the yttria particles contained as a dispersion within PM2000, prove to have good radiation resistance. The dpa dose of 0.33, and the 4000 appm He being introduced into the particles, do not change the structure of yttria, although the surrounding matrix is clearly damaged (see [7]). With their important role as pinning points for dislocations, and with their stability under radiation condition, these particles should be able to maintain the material creep properties.

Acknowledgements

The authors are thankful to Max Döbeli, who performed the He implantation at the Swiss Federal Institute of Technology, to Tomislav Revac at the Paul Scherrer Institute for the sample preparation. The work was partially supported by the EU projects RAPHAEL and EXTREMAT.

References

[1] C. Degueldre, S. Conradson, W. Hoffelner, Comp. Mater. Sci. 33 (2005) 3.
[2] A. Czyrska-Filemonowicz, B. Dubiel, J. Mater. Process. Technol. 64 (1997) 53.
[3] Dispersion-Strengthened High-Temperature Materials/ Material properties and applications, Prospectus from Plansee, 2003, 706 DE.04.03(1000)RWF.
[4] O.N. Carlson, Bull. Alloy Phase Diagr. 11 (1) (1990) 61.
[5] M. Klimiankou, R. Lindau, A. Möslang, J.A. Schröder, Powder Metall. B 48 (3) (2005) 277.
[6] M.A. Pouchon, M. Döbeli, R. Schelldorfer, J. Chen, W. Hoffelner, C. Degueldre, in: Proc. of 16th International

Conference on Physics of Radiation Phenomena and Radiation Material Science (Alushta, Crimea, 3–7 September, 2004), (VANT, Voprosy Atomnoi Nauki i Techniki, ISSN 1562–6016), vol. 3, 2005, p. 122.
[7] M.A. Pouchon, J. Chen, M. Döbeli, W. Hoffelner, J. Nucl. Mater. 352 (2006) 57.
[8] ASTM Designation: E 521 – 96, Neutron Radiation Damage Simulation by Charged-Particle Irradiation, 1996.
[9] J.F. Ziegler, J.P. Biersack, U. Littmark (Eds.), The Stopping and Range of Ions in Solids, Pergamon, New York, 1985.
[10] V.G. Bhide, N.V. Bhat, J. Chem. Phys. 48 (7) (1968) 3103.
[11] B. Ravel, M. Newville, J. Synchrotron Rad. 12 (2005) 537.